scientific reports

Check for updates

OPEN

Integration of multi-omics and single-cell analysis reveals ZBP1 as a prognostic biomarker of renal cell carcinoma

Changhua Li[1,4], Jusen Nong[3,4], Yong Li[3], Congjun Wang[3], Wenhao Lu[2], Bo Shi[3]✉ & Cheng Su[3]✉

Z-DNA binding protein 1 (ZBP1) is a critical factor that induces various forms of cell death and inflammatory responses. However, it has not been comprehensively analyzed in malignancies. The present study aimed to elucidate the oncogenic role of ZBP1 in human malignancies and examine its prospective function in renal cell carcinoma. The pathogenic significance of ZBP1 in malignancies was clarified using a multi-omics analysis and single-cell analysis utilizing bioinformatics methods. The function of ZBP1 in renal cell carcinoma was validated using in vivo and in vitro studies. In this study, we proved that ZBP1 high expression was significantly correlated with worse prognosis in kidney renal clear cell carcinoma and acute myeloid leukemia. Elevated ZBP1 levels correlated with cancer-associated fibroblast invasion. Furthermore, the single-cell analysis revealed that ZBP1 was significantly expressed in CD4+ T cells, CD8+ T cells, and regulatory T cells. ZBP1 may participate in cancer by regulating the inflammatory pathways. Cellular tests demonstrated that downregulating ZBP1 expression significantly inhibited renal cell carcinoma cell proliferation, migration, and invasion. The transplanted tumor model indicated that suppressing ZBP1 expression significantly reduced tumor progression. ZBP1 is a promising biomarker related to the prognosis of pan-cancer, especially renal cell carcinoma.

Keywords ZBP1, Renal cell carcinoma, Proliferation, Tumor microenvironment

Z-DNA binding protein 1 (ZBP1), alternatively termed DAI or DDLM-1, is a key mediator of DNA-triggered innate immunity[1]. Structurally, its N-terminal region harbors two Z-nucleic acid binding domains (Zα1/Zα2), while the central segment contains dual RIP homo-interaction motifs (RHIM) 1 and 2. These domains facilitate the production of type I interferons (IFN) and pro-inflammatory cytokines upon interaction with B-DNA or pathogen-derived nucleic acids[2,3]. Notably, ZBP1 not only acts as a viral RNA receptor, but also induces necroptosis and inflammatory cascades[4–6]. Intriguingly, its regulation of type I IFN operates independently of RIPK1–RIPK3–MLKL-mediated necroptosis or caspase-8-dependent apoptosis, suggesting a distinct mechanistic pathway[7]. Beyond viral infections, ZBP1 is implicated in diverse pathologies, such as SARS-CoV-2 complications, dermatological inflammation, cardiac dysfunction, and oncogenesis[8–11].

Emerging evidence highlights ZBP1-driven necroptosis as a novel modulator of tumor immunogenicity, which is suppressed by ADAR1 activity. Targeting this pathway presents a therapeutic strategy to overcome immune checkpoint resistance in malignancies[12]. Furthermore, experimental models underscore the role of ZBP1 in promoting tumor necrosis and metastasis, with its ablation significantly curtailing these processes[13]. Despite its emerging significance, pan-cancer analyses correlating ZBP1 expression with clinical outcomes remain limited. To address this gap, we used multi-omics databases to systematically explore the expression patterns, prognostic relevance, and functional influence of ZBP1 across cancers. Combined with in vitro and in vivo validation in renal cell carcinoma (RCC), our results elucidate ZBP1 is a promising biomarker in RCC.

[1]Department of Emergency, The First Affiliated Hospital of Guangxi Medical University, Nanning, China. [2]Guangxi Medical University, Nanning, China. [3]Department of Pediatric Surgery, The First Affiliated Hospital of Guangxi Medical University, Nanning, China. [4]Changhua Li and Jusen Nong have Contributed equally. ✉email: shibo893210@163.com; sc8338651@gmail.com

Results

Gene expression analysis

TCGA data demonstrated that ZBP1 expression was high in 10 tumor tissues (BRCA, ESCA, HNSC, KIRC, KIRP, LUAD, UCEC, CESC, CHOL, and GBM; Fig. 1A). Normal tissues from the GTEx dataset were used as controls to assess the disparity in ZBP1 expression between normal tissues and DLBC, LAML, OV, TGCT, and THYM tumor tissues (Fig. 1B). The CPTAC data demonstrated that total ZBP1 protein expression was elevated in LUAD and UCEC tissues compared to normal tissues, but was decreased in LIHC and ovarian cancer tissues (Fig. 1C). ZBP1 expression was associated with the pathogenic phases of ACC, HNSC, KIRC, and LUAD (Fig. 1D). IHC analysis of our clinical samples demonstrated increased ZBP1 protein expression in the RCC samples (Fig. S1).

Survival analysis

The relationship between ZBP1 expression and the prognosis of patients with different cancers was analyzed using TCGA and Gene Expression Omnibus (GEO) data. The results demonstrated that elevated ZBP1 expression was correlated with reduced OS in patients with KIRC and LAML (Fig. 2A), and was correlated with reduced DFS in patients with DLBC and LGG (Fig. 2B). Decreased ZBP1 expression was correlated with decreased OS in patients with HNSC, and with decreased DFS in patients with CHOL. Furthermore, decreased ZBP1 expression was correlated with decreased OS and DFS in patients with LIHC and SKCM.

Genetic alteration analysis

ZBP1 exhibited the greatest mutation frequency (>8%) in colorectal cancer, mostly characterized by "mutation", with around 7% associated with the "amplification" variant of CNA (Fig. 3A). Figure 3B presents more detail on the types, loci, and case of ZBP1 gene alterations. The primary mutation location in the ZBP1 gene was P278, situated in the non-functional area, and was identified in five tumors (SKCM, n = 2; LUAD, n = 1; and sarcoma, n = 1) (Fig. 3B). Furthermore, OS, disease-specific survival, DFS, and progression-free survival were not different between the patients with LUAD and sarcoma, irrespective of ZBP1 alterations (Fig. 3C).

Immune infiltration analysis

As critical constituents of the TME, tumor-infiltrating immune cells are intricately associated with cancer initiation, progression, and metastatic dissemination[14,15]. Within this stromal niche, CAFs (Cancer-Associated Fibroblasts) modulate the functional states of diverse immune populations[16,17]. Using TCGA datasets, we systematically interrogated correlations between ZBP1 expression and immune infiltration patterns across malignancies. Notably, ZBP1 levels were significantly and positively associated with CAF infiltration scores in COAD, LGG, PAAD, and READ, while demonstrating an inverse relationship in BRCA cohorts (Fig. 4).

Enrichment analysis of ZBP1-related partners

We used STRING to identify 35 proteins that can interact with ZBP1 and created the interaction network of these proteins (Fig. 5A). We identified the 100 most closely associated genes correlated with ZBP1 expression via GEPIA2, based on TCGA tumor gene expression data. The ZBP1 expression level was positively correlated with CMPK2, IRF7, OAS1, SAMD9L, and PARP12 (all, $P < 0.01$) (Fig. 5B). In most of the cancer types, ZBP1 and the aforementioned five genes were positively correlated (Fig. 5C). Studies of the overlap of the two groups identified a common member: IRF7 (Fig. 5D). The integrated KEGG enrichment analysis of the two datasets indicated that ZBP1 may affect tumor initiation and progression via the NOD-like receptor signaling pathway (Fig. 5E).

Single-cell analysis of *ZBP1* expression distribution in pan-cancer

The TISCH database integrates large-scale scRNA-seq data with cell type-resolved transcriptomic annotations, enabling systematic interrogation of the TME across 27 cancer types and 76 tumor cohorts. Through Uniform Manifold Approximation and Projection (UMAP) dimensionality reduction (Fig. 6A), we mapped ZBP1 transcriptional profiles at single-cell resolution, followed by quantitative assessment of its expression heterogeneity using violin plot analysis (Fig. 6B). Notably, ZBP1 enrichment was pronounced in immunomodulatory T-cell subsets, including CD4+ helper T cells, CD8+ cytotoxic T lymphocytes, and regulatory T cells (Tregs).

Effects of knocking down ZBP1 on renal cell carcinoma cell proliferation, invasion, and migration

Three types of siRNA that suppressed ZBP1 expression were transfected into 786-O and CAKI-2 cells, and their inhibitory efficacy was assessed. The western blot analysis indicated that siZBP1-1 dramatically reduced ZBP1 protein expression relative to the control (Fig. 7A). Hence, siZBP1-1-transfected cells were chosen for further experimentation. The CCK-8 and clonal formation experiments demonstrated that knocking down ZBP1 suppressed 786-O and CAKI-2 cell proliferation (Fig. 7B, C). The scratch healing assays demonstrated that downregulating ZBP1 expression inhibited the migration of both cell lines (Fig. 7D, E). Subsequently, the Transwell assays demonstrated that knocking down ZBP1 reduced cell invasion and migration (Fig. 7F, G).

ZBP1 knockdown suppresses tumor growth *in vivo*

The in vitro cell experiment results revealed that ZBP1 has a contributing function in renal cell carcinoma. We further assessed the effects of knocking down ZBP1 on tumor growth in vivo. We developed transplanted tumor models in nude mice and assessed the progress of the transplanted tumors (Fig. 8A, B). The ZBP1 knockdown group had significantly reduced tumor weight and size in comparison to the control group (Fig. 8C, D). The maximum diameter of the transplanted tumors in the ZBP1 gene knockdown group was 5.0 ± 0.8 (mm), and in the control group was 13.0 ± 2.6 (mm).

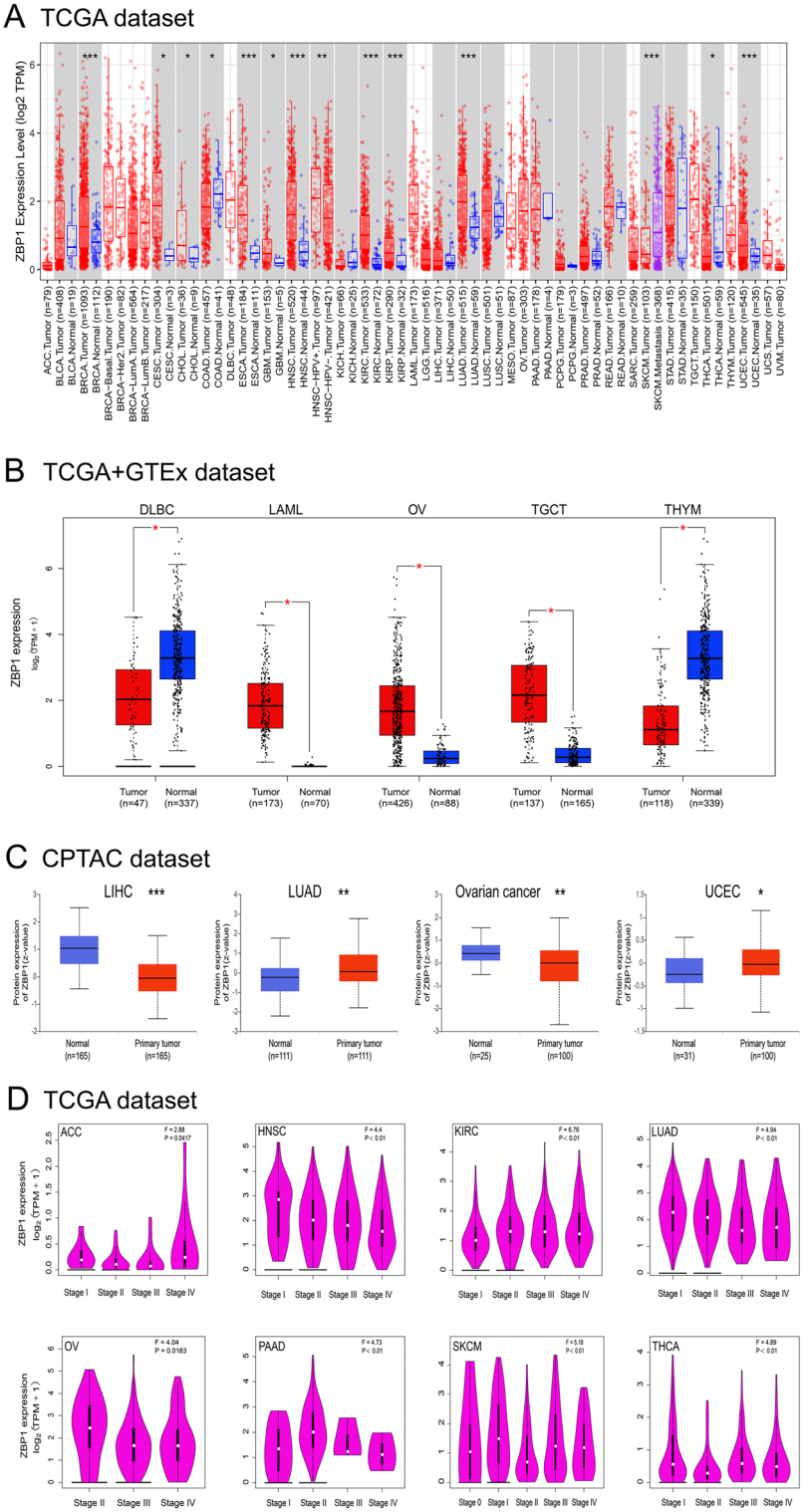

Fig. 1. Expression level of ZBP1 gene in different tumors and pathological stages. (**A**) The expression status of the ZBP1 gene in different cancers or specific cancer subtypes was analyzed through TIMER2. (**B**) For the type of DLBC, LAML, OV, TGCT and THYM in the TCGA project, the corresponding normal tissues of the GTEx database were included as controls. The box plot data were supplied. (**C**) The expression level of ZBP1 total protein between normal tissue and primary tissue of LIHC, LUAD, Ovarian cancer and UCEC. (**D**) Evaluate the correlation between the expression of ZBP1 and the pathological stages of ACC, HNSC, KIRC, LUAD, OV, PAAD, SKCM and THCA by using the GEPIA2. (*$p < 0.05$; **$p < 0.01$; ***$p < 0.001$).

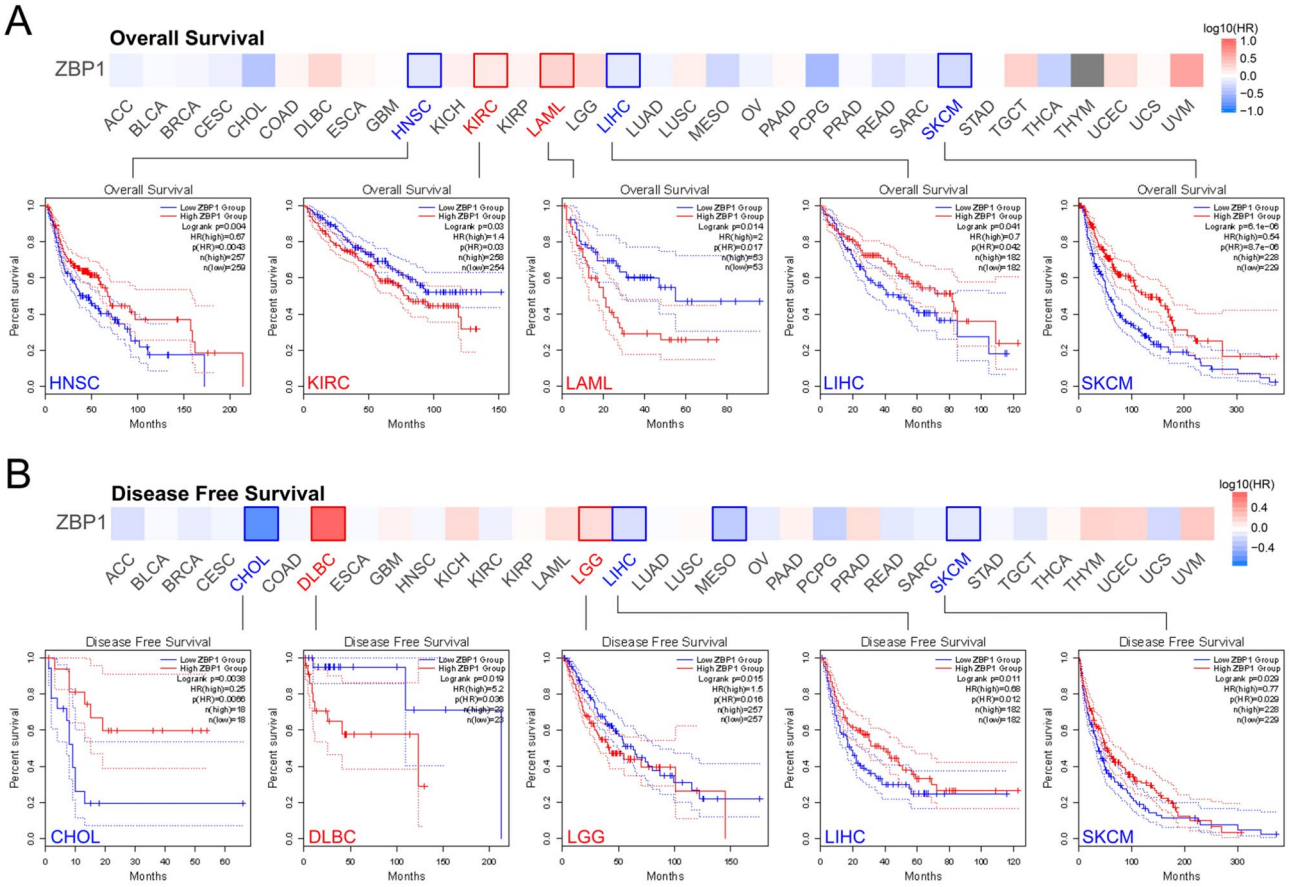

Fig. 2. Correlation between ZBP1 gene expression and survival prognosis of cancers in TCGA. GEPIA2 was used to evaluate the relationship between ZBP1 gene expression and overall survival (**A**) and disease-free survival (**B**) in all TCGA tumors.

Discussion

ZBP1 functions as a pattern recognition receptor that detects Z-DNA/RNA structures during viral infection, initiating diverse cell death modalities (e.g., necroptosis) and inflammatory signaling[18]. While its role in viral immunity, specifically influenza A virus pathogenesis, is well characterized, its implications in oncology remain underexplored.

This study and several previous works have observed that ZBP1 exhibits biphasic prognostic value in various cancer types, and the underlying mechanism may stem from the biological diversity of cancer. Firstly, there is a crucial functional balance downstream of ZBP1 activation: on one hand, it effectively induces immunogenic cell death, directly killing tumors and activating T-cell responses[19–21]; on the other hand, ZBP1 signals may preferentially activate pro-inflammatory pathways, creating a chronic inflammatory and immunosuppressive microenvironment[22]. Secondly, the genetic background and origin of tumor cells determine their internal signaling networks, which may 'reprogram' the output of ZBP1's function. For example, in colorectal cancer, ZBP1 mainly exerts tumor-suppressive effects[23]; while in triple-negative breast cancer, the downregulation of ZBP1 is associated with increased genomic instability, immunosuppression, and poor patient prognosis[24]. Finally, the immune composition of the tumor microenvironment is also a decisive factor. A functional immune system can amplify the benefits of immunogenic death induced by ZBP1, while an immunosuppressive environment may dominate its pro-tumor effects. Therefore, the role of ZBP1 in tumor diseases must be comprehensively interpreted in conjunction with its molecular and immune context.

The complex biological environment around tumor cells, known as the TME, mainly comprises immune cells, extracellular matrix, and other internal and external substances. The interaction between tumors and the TME is particularly complex, and the TME of different tumors exhibits immunological heterogeneity[25,26]. In the present study, the TIMER2.0 analysis revealed a substantial association between ZBP1 expression and CAF infiltration across multiple cancer types. Furthermore, single-cell analysis demonstrated that ZBP1 exhibited considerable expression levels in CD4+ T cells, CD8+ T cells, and Tregs. This result facilitates a more comprehensive understanding of the correlation between ZBP1 expression and various immune cells in the TME. CAFs are critical elements of the TME that release cytokines that facilitate tumor angiogenesis and induce epithelial–mesenchymal transition (EMT) in tumor cells, enhancing the suitability of the milieu for tumor proliferation[27,28]. Tregs directly regulate innate immune system activity by interacting with mononuclear phagocytes, granulocytes, dendritic cells, and innate lymphocytes, affecting both autoimmune and non-

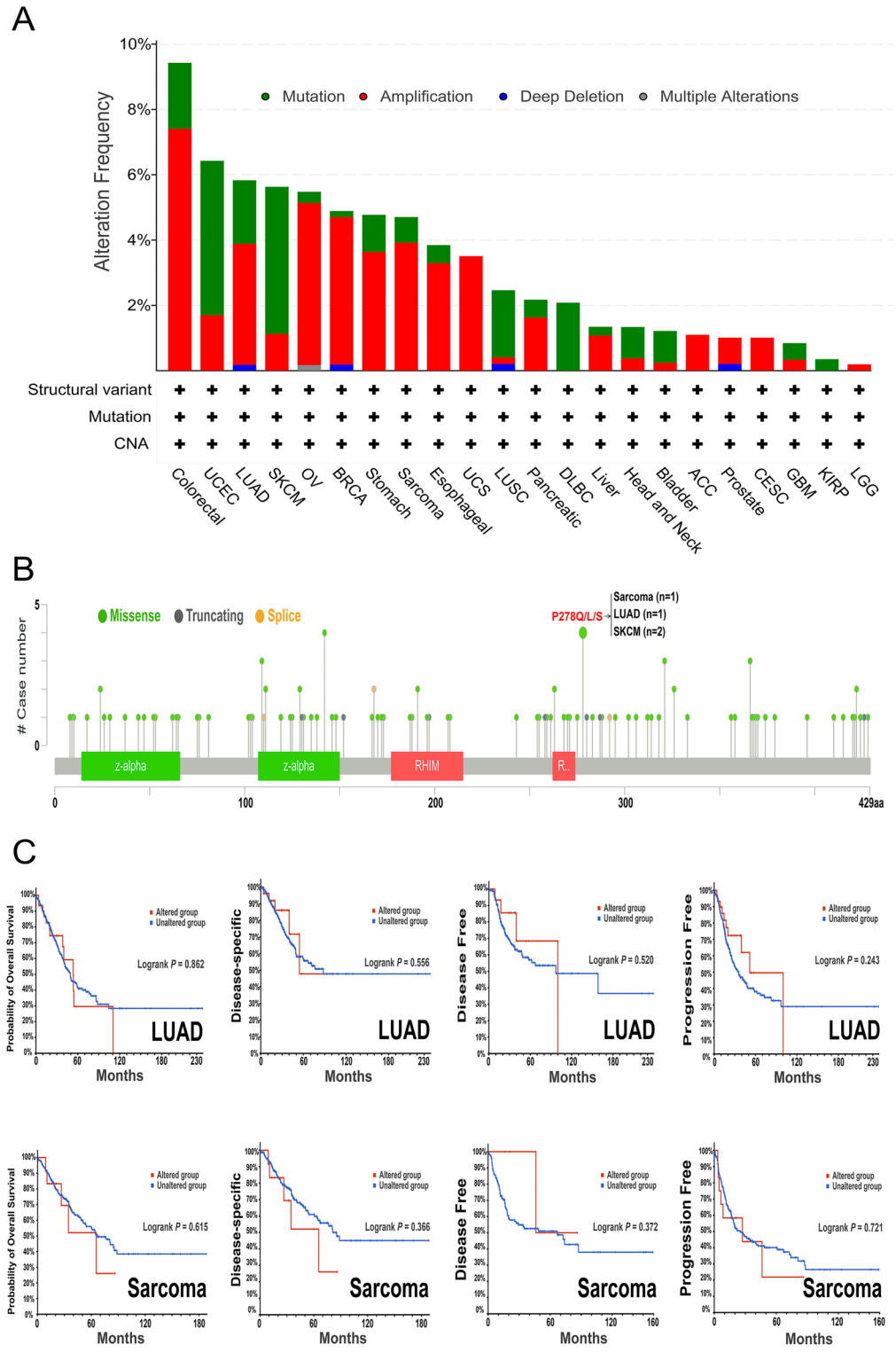

Fig. 3. Mutation feature of ZBP1 in different tumors of TCGA. The cBioPortal tool was employed to analyze the mutation features of ZBP1 in the TCGA tumors. The mutation type (**A**) and mutation site (**B**) are used to represent the frequency of alteration. We also used the cBioPortal tool for analyzing the potential correlation between mutation status and the overall, disease-specific, disease-free, and progression-free survival of LUAD and Sarcoma (**C**).

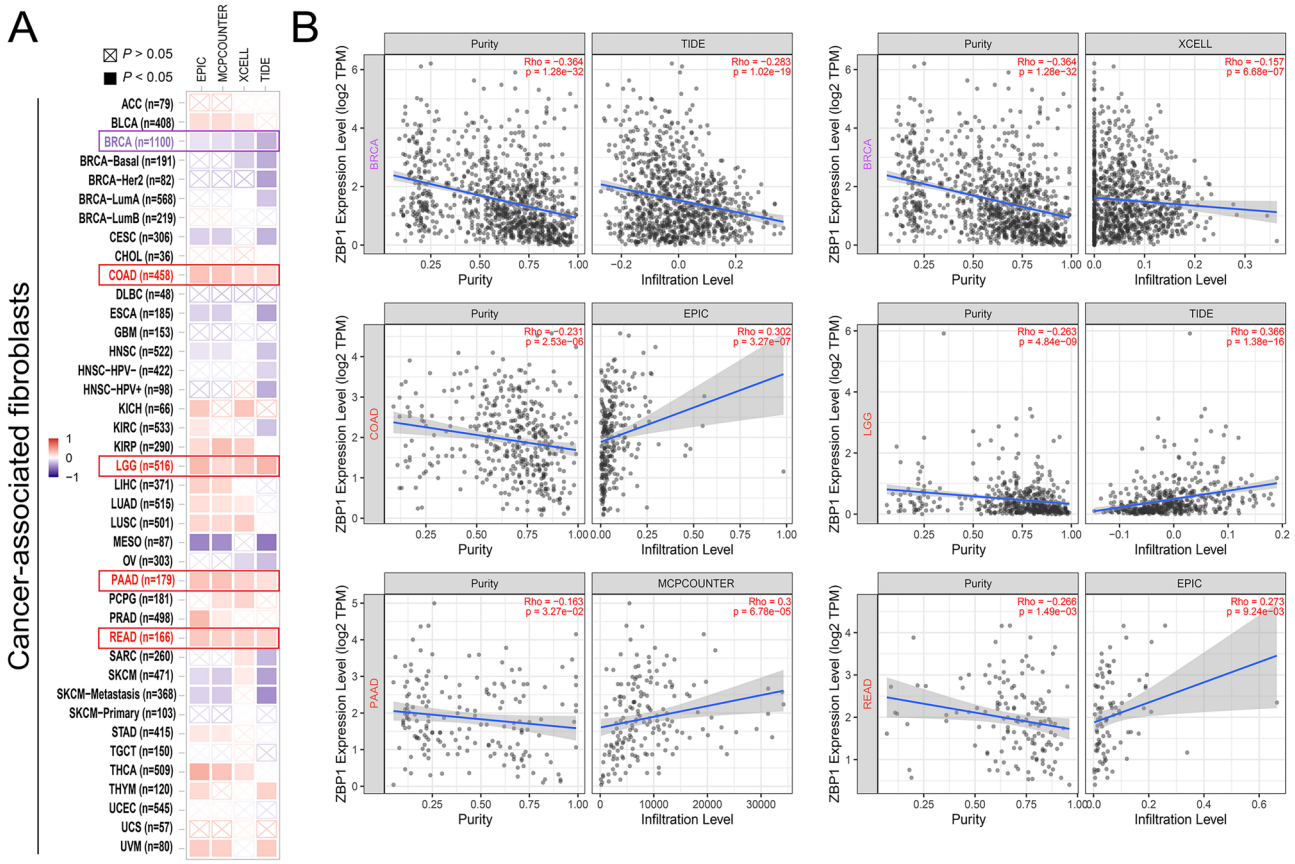

Fig. 4. Correlation analysis between ZBP1 expression and immune infiltration of cancer-associated fibroblasts. (**A**) The thermogram represents the relationship between cancer-associated fibroblasts and the expression of the ZBP1 gene in all cancers. (**B**) The scatter plot represents the relationship between CAFs infiltration and ZBP1 gene expression in BRCA, COAD, LGG, PAAD, and READ.

autoimmune inflammation. It primarily influences cell viability, proliferation, cytokine synthesis, phagocytosis, cytotoxicity, and the modulation of other effector activities[29,30]. ZBP1 is a crucial receptor that initiates cellular inflammation and may influence the functionality of TME immune cells by modulating the inflammatory response, facilitating carcinogenesis and progression. However, the precise molecular mechanism requires additional investigation.

We included data on ZBP1 binding components and the genes linked to ZBP1 expression across all cancers, which revealed a robust correlation between the expression of five genes (CMPK2, IRF7, OAS1, PARP12, and SAMD9L) and ZBP1 expression in the majority of the cancers. CMPK2, IRF7, and OAS1 are essential components in the cellular inflammatory response[31–33]. Tumor-associated inflammation can facilitate tumor advancement by enhancing angiogenesis and metastasis, undermining anti-tumor immune responses and altering tumor cell susceptibility to chemotherapeutic agents. A persistent, uncontrollable inflammatory microenvironment can induce tumorigenesis by activating gene alterations[34]. The KEGG enrichment analysis revealed the possible role of the NOD-like receptor signaling pathway in cancer etiology or pathophysiology. *Fusobacterium nucleatum* activates NF-κB via the NOD1–RIPK2 pathway in esophageal cancer, resulting in tumor development[35]. In colon cancer, the release of the proinflammatory cytokine IL-1β is triggered by the activation of the NLRP3 inflammasome in macrophages. IL-1β influences EMT and promotes colorectal cancer cell invasion and migration[36,37], corroborating our gene enrichment analysis results.

The precise molecular mechanism by which ZBP1 affects tumor formation via inflammatory pathways in cancer requires further investigation. We successfully identified the effector molecule IRF7, which may be closely related to ZBP1. Interferon regulatory factor 7 (IRF7) is a member of the interferon regulatory factor (IRF) family. Activating IRF7 can inhibit various viral and bacterial infections, suppress the growth and metastasis of certain cancers, but it may also affect the tumor microenvironment and promote the development of other cancers[32]. Additionally, IRF7 is closely related to the inflammatory pathway[38]. The exact mechanism between ZBP1, IRF7 and the inflammatory pathway deserves further in-depth study, which provides a clear direction for our subsequent research.

The present study demonstrated that knocking down ZBP1 markedly decreased renal cell carcinoma cell proliferation, invasion, and migration. Moreover, the in vivo xenotransplantation models demonstrated that ZBP1-knockdown 786-O cells exhibited reduced growth, corroborating the in vitro results. Nevertheless, the present study was subject to the following limitations. The sample size for some uncommon tumor types is

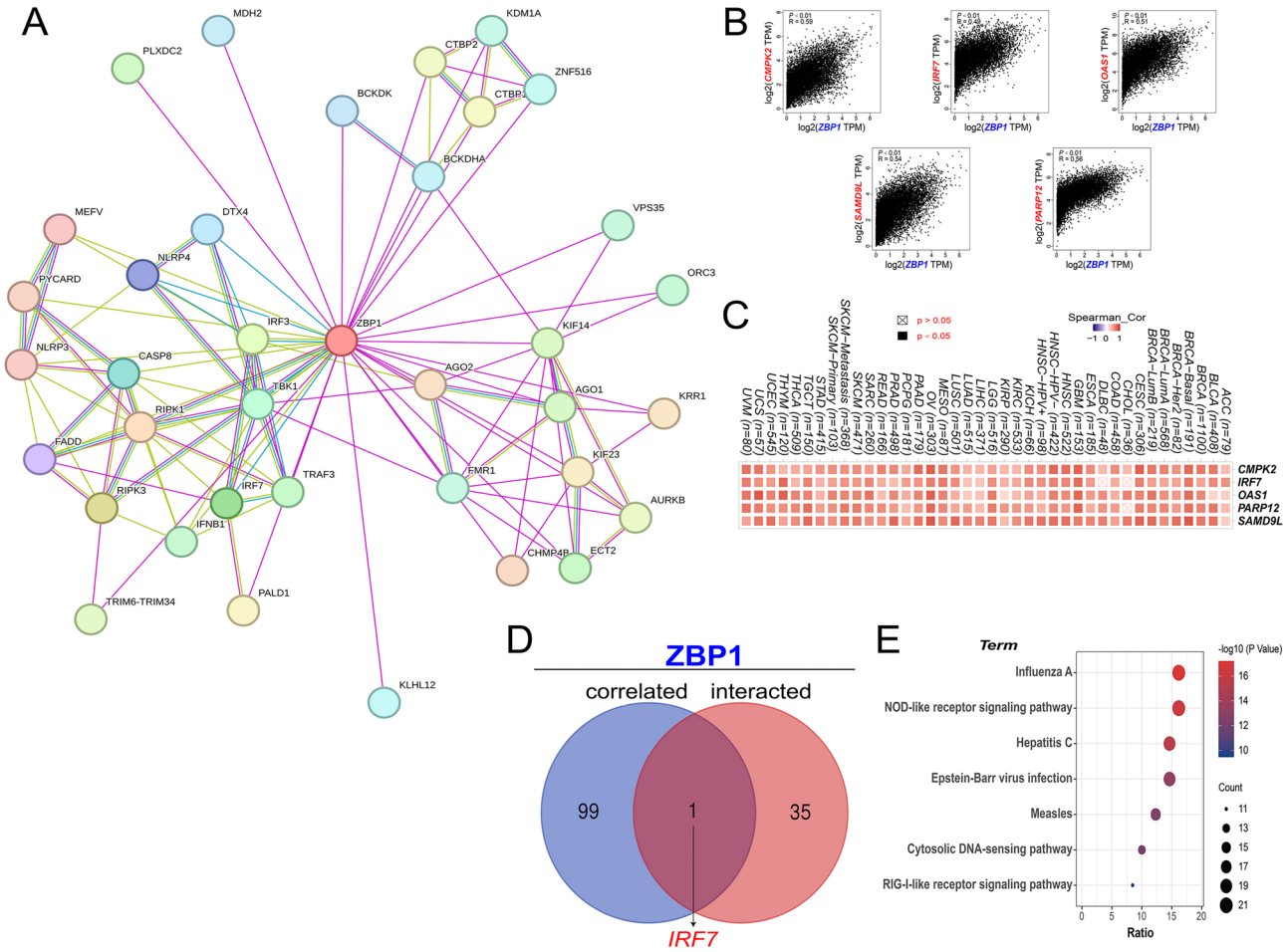

Fig. 5. Enrichment analysis of ZBP1-related genes. (**A**) ZBP1 protein interaction network diagram. (**B**) The scatter plot of ZBP1-related top 5 genes. (**C**) The expression of correlation between cross-genes and ZBP1 in pan-cancer. (**D**) Cross-analysis of ZBP1-related genes and ZBP1-binding genes. (**E**) KEGG enrichment analysis based on ZBP1-related and ZBP1-binding genes.

rather small; hence, it is crucial to validate larger datasets to improve the accuracy of the analysis. Furthermore, although we have confirmed the expression of ZBP1 in clinical samples, the current sample size is limited. In the future, we still need to collect more tumor samples and, in combination with the prognosis of the patients, analyze the clinical relevance of ZBP1.

Methods

Gene expression analysis

Differences in ZBP1 expression between tumors and adjacent normal tissues in various cancer types from The Cancer Genome Atlas (TCGA) project were identified using the Gene_DE module of Tumor Immune Estimation Resource, version 2 (TIMER2.0), when providing the data, this platform has uniformly normalized the original counts into Log_2[TPM (Transcripts per million)] values. Then, the Wilcoxon rank sum test was used to compare the expression levels in tumor and normal tissues. A *p*-value less than 0.05 was considered to indicate a statistically significant difference. By default, no multiple test correction across cancer types is performed. It shows the individual p-values for each cancer type. For tumors lacking normal tissue, box plots of expression differences between these tumor tissues and Genotype-Tissue Expression Project (GTEx) (genotype) tissues were obtained through the Expression Analysis - Box Plots module of Interactive Analysis of Gene Expression Profiles, version 2 (GEPIA2) web server[39], this platform has uniformly normalized the original counts to log_2(TPM+1) values. ZBP1 expression across diverse pathological stages of all TCGA cancers was explored using the GEPIA2 Pathological stage map module, Log_2(TPM +1) transformed expression data were used for box or violin plots. ZBP1 protein expression in tumor and normal tissues from Clinical Proteomic Tumor Analysis Consortium (CPTAC) data was analyzed using UALCAN[40].

Survival prognosis analysis

The significance map data of overall survival (OS) and disease-free survival (DFS) for ZBP1 across all TCGA tumors was obtained using the GEPIA2 Survival map module. The platform used the Log-rank test to compare

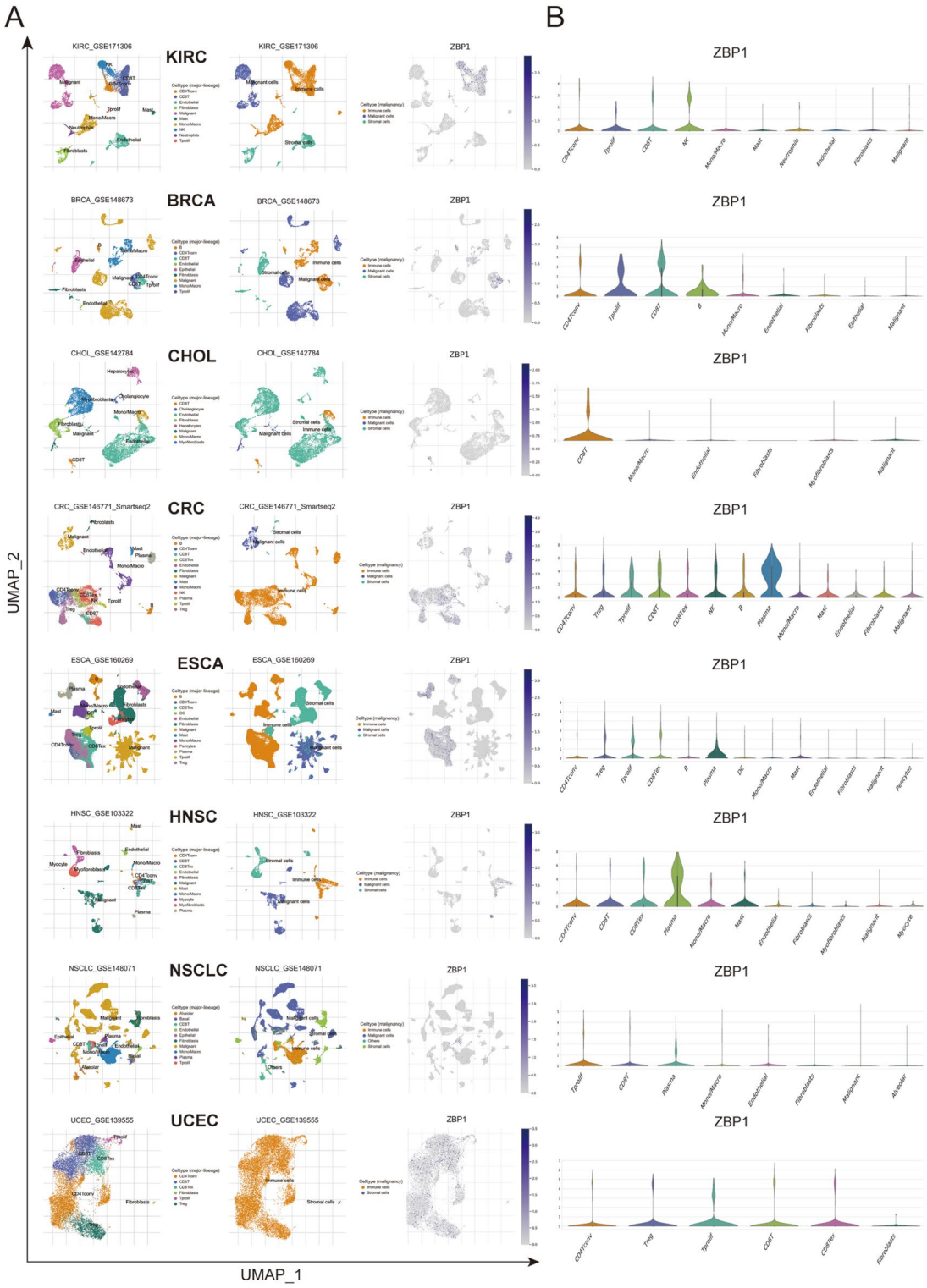

Fig. 6. Single-cell analysis of ZBP1 expression characteristics across pan-cancer. (**A**) The visualized single-cell UMAP plot displays the distribution of different cell types (left) and the expression of ZBP1 (right) within the pan-cancer single-cell dataset. (**B**) The violin plot quantifies the distribution of ZBP1 expression across different cell types in pan-cancer.

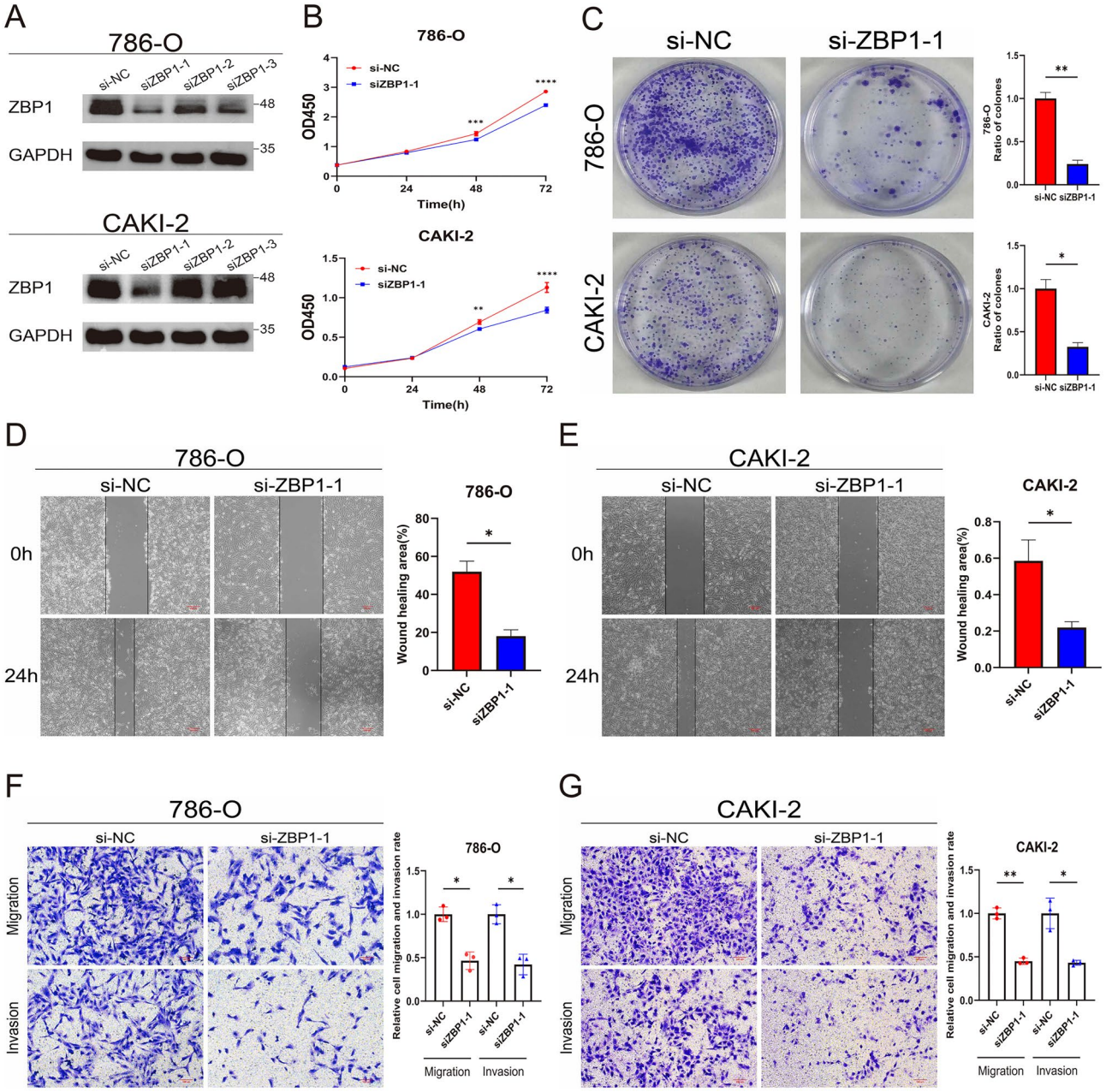

Fig. 7. ZBP1 contributed to the proliferation, migration and invasion of renal cell carcinoma in vitro. (**A**) The ZBP1 protein expression (western blot) in 786-O and CAKI-2 knockdown cells compared with control 786-O and CAKI-2 cells. (**B**) CCK8 assays of 786-O and CAKI-2 cells in control and ZBP1-knockdown group. (**C**) The plate clone formation experiment and ratio of clones of 786-O and CAKI-2 cells in control and ZBP1-knockdown group. (**D** and **E**) Cell scratch assay of 786-O and CAKI-2 cells in control and ZBP1-knockdown group. (**F** and **G**) Transwell assay of 786-O and CAKI-2 cells in control and ZBP1-knockdown group. (*$p <$ 0.05; ** $p < 0.01$; *** $p < 0.001$; **** $p < 0.0001$).

the survival differences between the high-expression group and the low-expression group, and presented the hazard ratio and the unadjusted *p*-value in the figure. The high and low expression groups were classified using a 50% high cut-off value and a 50% low cut-off value, respectively.

Genetic alteration analysis

ZBP1 gene alterations in all TCGA malignancies, encompassing mutation frequency, mutation type, and copy number alterations (CNA), were examined using cBioPortal[41,42]. The disease-free, progression-free, and disease-specific survival of TCGA patients with cancer with or without *ZBP1* gene alteration were likewise compared.

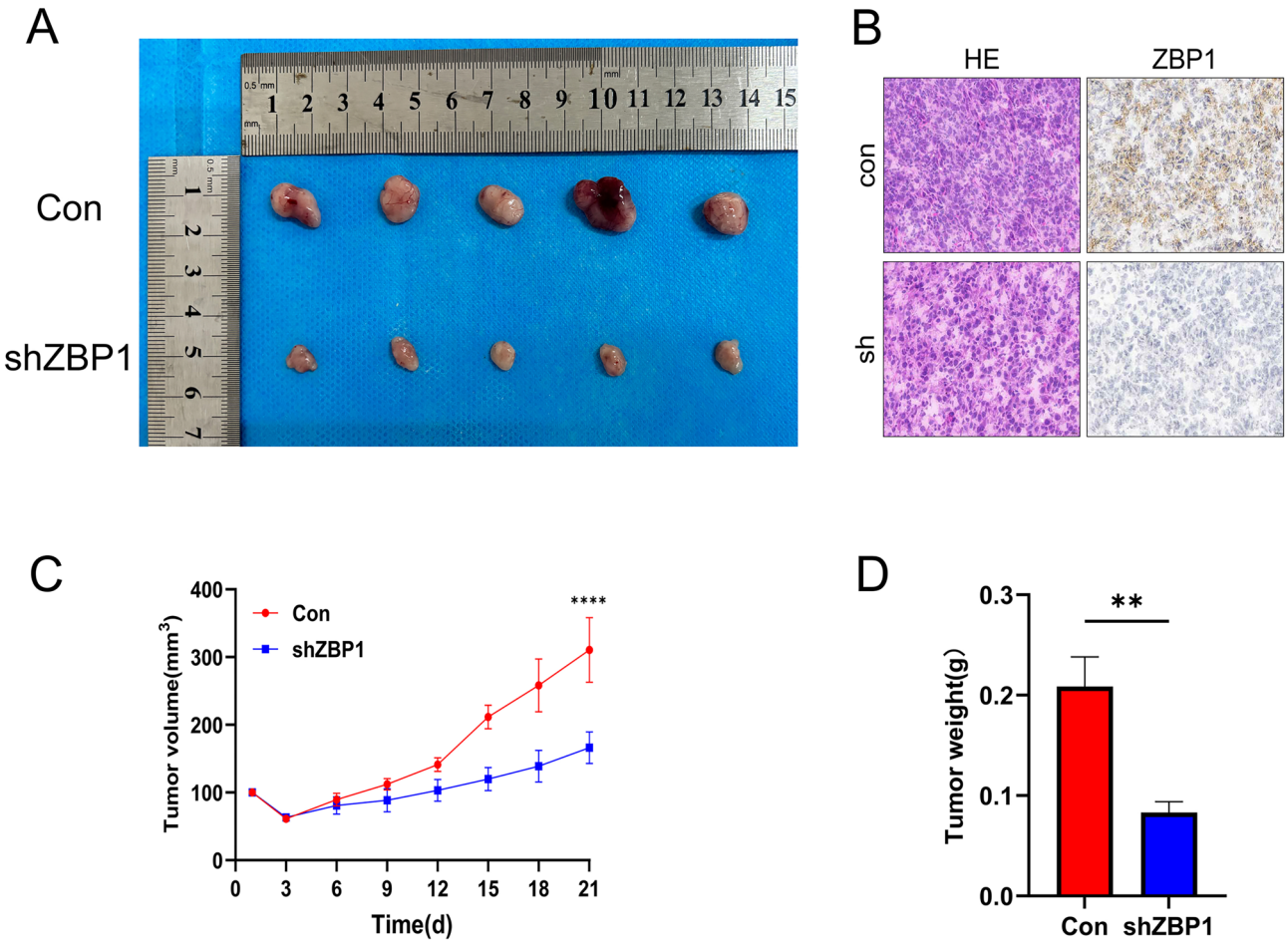

Fig. 8. Knockdown of ZBP1 inhibits renal cell carcinoma cell tumorigenesis in vivo. (**A**) The appearance of nude mice from 786-O Con and shZBP1 groups (n = 5). (**B**) Tumor size of the two groups. (**C**) Tumor images of nude mice in the two groups. (**D**) Weight of tumors in the two groups. (**$p < 0.01$).

Immune infiltration analysis

The expression of ZBP1 and immune infiltrates in all TCGA tumors was analyzed using the TIMER2.0 web server Immune-Gene module. Cancer-associated fibroblasts (CAFs) were selected as the immune infiltrates. Immune infiltration was assessed using the TIMER, CIBERSORT, CIBERSORT abs, quanTIseq, xCell, MCPcounter, and EPIC algorithms.

ZBP1-related gene enrichment analysis

Experimentally verified ZBP1 binding proteins were identified using STRING (https://string-db.org/). By leveraging all TCGA tumor and normal tissue datasets, the GEPIA2 Similar Gene Detection module was used to discover the top 100 target genes associated with ZBP1. Pearson correlation analysis between ZBP1 and the selected genes was performed using the GEPIA2 Correlation analysis module. Heat map data for specific genes was obtained using the TIMER2.0 Gene_Corr module. ZBP1 binding proteins and the related genes were cross-analyzed using jvenn[43]. We performed Kyoto Encyclopedia of Genes and Genomes (KEGG) pathway analysis on the data[44], using DAVID for functional annotation graph data, while the R packages tidyr and ggplot2 displayed the enriched pathways.

Single-cell analysis

Single-cell RNA-seq data analyzed in this study were obtained from the Tumor Immune Single-Cell Hub 2 (TISCH2) database[45]. The TISCH2 resource provides uniformly processed tumor microenvironment datasets, which undergo a standardized pipeline encompassing quality control, batch effect correction, cell clustering, differential expression analysis, and multi-level cell type annotation. Specifically, cell identities are assigned through the identification of highly expressed genes within individual clusters and their systematic comparison against established cell marker databases. All visualizations presented herein are derived directly from these pre-processed and annotated data.

Cell culture

Human renal cell carcinoma cell lines 786-O and CAKI-2 were obtained from Wuhan Pricella Biotechnology Co., Ltd. (China). The 786-O cells were cultivated in RPMI 1640 (Gibco, USA) containing 10% FBS (fetal bovine serum) (Gibco, USA). The CAKI-2 cells were cultured in a medium suitable for CAKI-2 cells (Pricella, Wuhan, China). The cell culture conditions were 37 °C with 5% CO_2. HANBIO (China) provided the small interfering RNA (siRNA) for the human target gene ZBP1, with the following sequences: siZBP1-1, F: 5′-GAUUCUGG AAGAAGAGCAATT-3′; R: 5′-UUGCUCUUCUUCCAGAAUCTT-3′; siZBP1-2, F: 5′-CAAUUAUUUACCAG CACAATT-3′; R: 5′-UUGUGCUGGUAAAUAAUUGTT-3′; siZBP1-3, F: 5′-GCUGGAUUUCCAUUGCAAAT T-3′; R: 5′-GCUGGAUUUCCAUUGCAAATT-3′. The 786-O and CAKI-2 cells were cultured in 6-well plates, then transfected using Lipofectamine™ 3000 (L3000075; Thermo Fisher Scientific) subsequent to cell walling.

Western blotting

Cell proteins were extracted using radioimmunoprecipitation assay (RIPA) lysis buffer (R0010, Solarbio, China). The protein concentration was determined using a bicinchoninic acid (BCA) Protein Assay Kit (Beyotime, China). Cell protein lysates were prepared with 5× sodium dodecyl sulfate (SDS) buffer and heat at 100 °C for 10 minutes before western blotting. Proteins were fractionated via SDS–polyacrylamide gel electrophoresis (SDS-PAGE) and subsequently transferred to a PVDF membrane. The membrane underwent 60-minute blocking with 5% bovine serum albumin (BSA) in Tris-buffered saline containing 0.05% Tween 20 (TBST). The membranes were incubated overnight at 4 °C with the primary antibodies [anti-GAPDH (60004-1-Ig, Proteintech, Wuhan, China), anti-ZBP1 (13285-1-AP, Proteintech, Wuhan, China)]. After TBST washing, the membranes were incubated for 60 minutes with the secondary antibodies, followed by an additional wash. An improved chemiluminescence detection kit (Thermo Fisher Scientific) and an automated image processing system (e-BLOT, China) revealed the PVDF membrane protein bands.

Colony formation assay

A 35-mm cell culture dish was injected with 1000 cells and cultured at 37 °C in 5% CO_2 for 2 weeks. After 30-minute fixation using 4% paraformaldehyde, the cells were stained with 0.1% crystal violet and subsequently photographed. Every experiment was repeated three times.

CCK-8 cell proliferation assay

Cell proliferation was examined using a Cell Counting Kit-8 (CCK-8) assay kit from Beyotime (C0037). In summary, 2×10^3 cells were inoculated onto 96-well plates with 100 μL complete medium. Subsequently, 90 μL culture medium and 10 μL CCK-8 solution were added to each well, and the plate was incubated for 1 hour in a cell incubator (37°C, incubation in the dark). The absorbance at 450 nm was quantified using a microplate reader (Thermo Fisher Scientific).

Scratch healing assay

Logarithmic growth-stage cells were cultivated in 6-well plates, then transfected subsequent to cell adhesion. Upon achieving 100% cell density, the cells were scratched using a 200-μL pipette tip, and the scratch healing was monitored microscopically at 0 and 24 hours. The experiments were conducted three times.

Transwell invasion and migration assay

Cells (200 μL) suspended in serum-free medium were transferred to the upper compartment of a Transwell chamber, followed by the addition of 500 μL complete medium to the lower chamber. The cells were cultured in a cell incubator for 48 hours, fixed in 4% paraformaldehyde for 20 minutes, and stained with 0.1% crystal violet. Three photographs were captured using a microscope for counting.

Nude mouse xenograft model

BALB/c nude mice (male, 4–5 weeks) were sourced and cared for by the Guangxi Medical University Animal Experiment Center. The animal experiments were approved by the Ethics Committee of the First Affiliated Hospital of Guangxi Medical University (approval number: 2024-D0291), and all methods were performed in accordance with the relevant guidelines and regulations, including the ARRIVE guidelines. The siZBP1-1 sequence was inserted into the PLv3-U6 expression vector. Viral vectors were obtained using Sun et al.'s viral transfection procedure[46]. The 786-O cells were grown in RPMI 1640 complete medium in flasks. Transfection efficiency was measured 72 hours after lentiviral transduction of shRNA-ZBP1 or control virus using a fluorescence microscope. The cells were subsequently grown for an additional 120 hours before implantation into nude mice. The 786-O cells (1×10^7 per animal) were injected into the right axilla of the nude mice. The nude mice were randomly selected, with five nude mice allocated to each group (n = 5). The size of the transplanted tumor was assessed using a caliper every 3 days. After 3 weeks, the rats were euthanized (the nude mice that were to undergo euthanasia were placed in a sealed box. A pre-mixed gas containing 40% CO_2 was introduced at a rate of 20% of the box volume per minute, causing the mice to gradually lose consciousness. Then, they were exposed to a lethal concentration (>70% CO_2) until their breathing and heartbeat ceased) and their appearance was photographed. The tumors were meticulously excised, weighed, and documented photographically. The comparison of tumor growth curves was conducted using repeated measures two-factor analysis of variance. The comparison of tumor weights among groups was performed using unpaired two-tailed Student's *t*-test. This study was reported in accordance with the ARRIVE guidelines (https://arriveguidelines.org).

Tissue specimens and immunohistochemistry (IHC) assays

Renal cell carcinoma (RCC) tissues were obtained from 6 patients who underwent nephrectomy at the First Affiliated Hospital of Guangxi Medical University between January and June 2025, while paired normal tissues were collected from these patients. The samples were maintained at −80°C. The present study was conducted in complete adherence to the principles of the Declaration of Helsinki. The study received approval from the First Affiliated Hospital of Guangxi Medical University Ethics Committee (Approval No. 2024-S770-01), all methods were performed in accordance with the relevant guidelines and regulations, including the Declaration of Helsinki.

ZBP1 protein levels were analyzed using 6 RCC samples. The RCC samples were fixed and paraffin-embedded according to standard protocols. The IHC analysis was performed using antibodies against ZBP1 (13285-1-AP, Proteintech, China). The IHC staining results were scored considering the staining intensity and the proportion of reaction-positive tumor cells. The staining intensity was scored as follows: 0, negative; 1, weak; 2, medium; and 3, strong. The frequency of positive cells was scored as follows: 0, <5%; 1, 1–25%; 2, 25–50%; 3, 50–75%; 4, >75%. Total scores of 0–12 were determined by multiplying the staining intensity score and the positive area score.

The nude mouse xenograft model tumor samples were fixed and paraffin-embedded according to standard protocols. The IHC analysis was performed using antibodies against ZBP1 (13285-1-AP, Proteintech, China).

Statistical analysis

The data are reported as the mean and standard error. Statistical comparisons were conducted using Student's *t*-tests. $P < 0.05$ indicated statistical significance. Each experiment was completed with a minimum of three repeats. The charts and graphics were created using the Prism 10 program.

Data availability

Availability of the data and materials, through public databases [TCGA (https://www.cancer.gov/ccg/research/genome-sequencing/tcga), GEO (https://www.ncbi.nlm.nih.gov/geo/), TISCH2 (https://tisch.compbio.cn/home/)] and analysis tools are outlined in the Methods section.

Received: 30 December 2025; Accepted: 23 March 2026
Published online: 11 April 2026

Reference

1. Kuriakose, T. & Kanneganti, T. D. ZBP1: Innate sensor regulating cell death and inflammation. *Trend. Immunol.* **39**, 123–134. https://doi.org/10.1016/j.it.2017.11.002 (2018).
2. Hao, Y. et al. ZBP1: A powerful innate immune sensor and double-edged sword in host immunity. *Int. J. Mol. Sci.* https://doi.org/10.3390/ijms231810224 (2022).
3. Oh, S. & Lee, S. Recent advances in ZBP1-derived PANoptosis against viral infections. *Front. Immunol.* **14**, 1148727. https://doi.org/10.3389/fimmu.2023.1148727 (2023).
4. Zhang, T. et al. Influenza virus Z-RNAs induce ZBP1-mediated necroptosis. *Cell* **180**, 1115-1129 e1113. https://doi.org/10.1016/j.cell.2020.02.050 (2020).
5. Kuriakose, T. et al. ZBP1/DAI is an innate sensor of influenza virus triggering the NLRP3 inflammasome and programmed cell death pathways. *Sci. Immunol.* https://doi.org/10.1126/sciimmunol.aag2045 (2016).
6. Kesavardhana, S. et al. ZBP1/DAI ubiquitination and sensing of influenza vRNPs activate programmed cell death. *J. Exp. Med.* **214**, 2217–2229. https://doi.org/10.1084/jem.20170550 (2017).
7. Jiao, H. et al. ADAR1 averts fatal type i interferon induction by ZBP1. *Nature* **607**, 776–783. https://doi.org/10.1038/s41586-022-04878-9 (2022).
8. Li, S. et al. SARS-CoV-2 Z-RNA activates the ZBP1-RIPK3 pathway to promote virus-induced inflammatory responses. *Cell. Res.* **33**, 201–214. https://doi.org/10.1038/s41422-022-00775-y (2023).
9. Devos, M. et al. Sensing of endogenous nucleic acids by ZBP1 induces keratinocyte necroptosis and skin inflammation. *J. Exp. Med.* https://doi.org/10.1084/jem.20191913 (2020).
10. Lei, Y. et al. Cooperative sensing of mitochondrial DNA by ZBP1 and cGAS promotes cardiotoxicity. *Cell* **186**, 3013-3032 e3022. https://doi.org/10.1016/j.cell.2023.05.039 (2023).
11. Enzan, N. et al. ZBP1 protects against mtDNA-induced myocardial inflammation in failing hearts. *Circ. Res.* **132**, 1110–1126. https://doi.org/10.1161/CIRCRESAHA.122.322227 (2023).
12. Zhang, T. et al. ADAR1 masks the cancer immunotherapeutic promise of ZBP1-driven necroptosis. *Nature* **606**, 594–602. https://doi.org/10.1038/s41586-022-04753-7 (2022).
13. Baik, J. Y. et al. ZBP1 not RIPK1 mediates tumor necroptosis in breast cancer. *Nat. Commun.* **12**, 2666. https://doi.org/10.1038/s41467-021-23004-3 (2021).
14. Rui, R., Zhou, L. & He, S. Cancer immunotherapies: Advances and bottlenecks. *Front. Immunol.* **14**, 1212476. https://doi.org/10.3389/fimmu.2023.1212476 (2023).
15. Bejarano, L., Jordão, M. J. C. & Joyce, J. A. Therapeutic targeting of the tumor microenvironment. *Cancer. Discov.* **11**, 933–959. https://doi.org/10.1158/2159-8290.CD-20-1808 (2021).
16. Biffi, G. & Tuveson, D. A. Diversity and biology of cancer-associated fibroblasts. *Physiol. Rev.* **101**, 147–176. https://doi.org/10.1152/physrev.00048.2019 (2021).
17. Kennel, K. B., Bozlar, M., De Valk, A. F. & Greten, F. R. Cancer-associated fibroblasts in inflammation and antitumor immunity. *Clin. Cancer Res.* **29**, 1009–1016. https://doi.org/10.1158/1078-0432.CCR-22-1031 (2023).
18. Zheng, M. & Kanneganti, T. D. The regulation of the ZBP1-NLRP3 inflammasome and its implications in pyroptosis, apoptosis, and necroptosis (PANoptosis). *Immunol. Rev.* **297**, 26–38. https://doi.org/10.1111/imr.12909 (2020).
19. Karki, R. & Kanneganti, T. D. ADAR1 and ZBP1 in innate immunity, cell death, and disease. *Trends Immunol.* **44**, 201–216. https://doi.org/10.1016/j.it.2023.01.001 (2023).
20. Wang, Q. et al. ZBP1 pathway promotes tumor immunogenicity in the combination of anti-HER2 therapy and epigenetic therapy. *Cell Rep.* **44**, 116314. https://doi.org/10.1016/j.celrep.2025.116314 (2025).
21. Nassour, J. et al. Telomere-to-mitochondria signalling by ZBP1 mediates replicative crisis. *Nature* **614**, 767–773. https://doi.org/10.1038/s41586-023-05710-8 (2023).
22. Yan, J., Wan, P., Choksi, S. & Liu, Z. G. Necroptosis and tumor progression. *Trends Cancer* **8**, 21–27. https://doi.org/10.1016/j.trecan.2021.09.003 (2022).

23. Műzes, G. & Sipos, F. PANoptosis as a two-edged sword in colorectal cancer: A pathogenic mechanism and therapeutic opportunity. *Cells* https://doi.org/10.3390/cells14100730 (2025).
24. Cho, M. G. et al. MRE11 liberates cGAS from nucleosome sequestration during tumorigenesis. *Nature* **625**, 585–592. https://doi.org/10.1038/s41586-023-06889-6 (2024).
25. Gong, Z. et al. Machine learning identifies TIME subtypes linking EGFR mutations and immune states in lung adenocarcinoma. *NPJ Digit. Med.* **8**, 796. https://doi.org/10.1038/s41746-025-02172-2 (2025).
26. Zhang, P. et al. Metabolic reprogramming signature predicts immunotherapy efficacy in lung adenocarcinoma: targeting SLC25A1 to overcome immune resistance. *Chin. J. Cancer Res.* **37**, 1000–1019. https://doi.org/10.21147/j.issn.1000-9604.2025.06.11 (2025).
27. Zhang, H. et al. Define cancer-associated fibroblasts (CAFs) in the tumor microenvironment: new opportunities in cancer immunotherapy and advances in clinical trials. *Mol. Cancer* **22**, 159. https://doi.org/10.1186/s12943-023-01860-5 (2023).
28. Liao, Z., Tan, Z. W., Zhu, P. & Tan, N. S. Cancer-associated fibroblasts in tumor microenvironment-accomplices in tumor malignancy. *Cell Immunol.* **343**, 103729. https://doi.org/10.1016/j.cellimm.2017.12.003 (2019).
29. Ou, Q., Power, R. & Griffin, M. D. Revisiting regulatory T cells as modulators of innate immune response and inflammatory diseases. *Front. Immunol.* **14**, 1287465. https://doi.org/10.3389/fimmu.2023.1287465 (2023).
30. Ohkura, N. & Sakaguchi, S. Transcriptional and epigenetic basis of Treg cell development and function: Its genetic anomalies or variations in autoimmune diseases. *Cell Res.* **30**, 465–474. https://doi.org/10.1038/s41422-020-0324-7 (2020).
31. Guan, X. et al. Microglial CMPK2 promotes neuroinflammation and brain injury after ischemic stroke. *Cell Rep. Med.* **5**, 101522. https://doi.org/10.1016/j.xcrm.2024.101522 (2024).
32. Qing, F. & Liu, Z. Interferon regulatory factor 7 in inflammation, cancer and infection. *Front. Immunol.* **14**, 1190841. https://doi.org/10.3389/fimmu.2023.1190841 (2023).
33. Liang, M. et al. OAS1 induces endothelial dysfunction and promotes monocyte adhesion through the NFκB pathway in atherosclerosis. *Arch. Biochem. Biophys.* **763**, 110222. https://doi.org/10.1016/j.abb.2024.110222 (2025).
34. Bi, Q. et al. Tumor-associated inflammation: The tumor-promoting immunity in the early stages of tumorigenesis. *J. Immunol. Res.* **2022**, 3128933. https://doi.org/10.1155/2022/3128933 (2022).
35. Nomoto, D. et al. *Fusobacterium nucleatum* promotes esophageal squamous cell carcinoma progression via the NOD1/RIPK2/NF-κB pathway. *Cancer Lett.* **530**, 59–67. https://doi.org/10.1016/j.canlet.2022.01.014 (2022).
36. Marandi, Y. et al. NLRP3-inflammasome activation is associated with epithelial-mesenchymal transition and progression of colorectal cancer. *Iran. J. Basic Med. Sci.* **24**, 483–492. https://doi.org/10.22038/ijbms.2021.52355.11835 (2021).
37. Deng, Q. et al. NLRP3 inflammasomes in macrophages drive colorectal cancer metastasis to the liver. *Cancer Lett.* **442**, 21–30. https://doi.org/10.1016/j.canlet.2018.10.030 (2019).
38. Chen, L. et al. NF-κB p65 and SETDB1 expedite lipopolysaccharide-induced intestinal inflammation in mice by inducing IRF7/NLR-dependent macrophage M1 polarization. *Int. Immunopharmacol.* **115**, 109554. https://doi.org/10.1016/j.intimp.2022.109554 (2023).
39. Tang, Z., Kang, B., Li, C., Chen, T. & Zhang, Z. GEPIA2: An enhanced web server for large-scale expression profiling and interactive analysis. *Nucleic Acids Res.* **47**, W556–W560. https://doi.org/10.1093/nar/gkz430 (2019).
40. Chen, F., Chandrashekar, D. S., Varambally, S. & Creighton, C. J. Pan-cancer molecular subtypes revealed by mass-spectrometry-based proteomic characterization of more than 500 human cancers. *Nat. Commun.* **10**, 5679. https://doi.org/10.1038/s41467-019-13528-0 (2019).
41. Unberath, P. et al. Searching of clinical trials made easier in cBioPortal using patients' genetic and clinical profiles. *Appl. Clin. Inform.* **13**, 363–369. https://doi.org/10.1055/s-0042-1743560 (2022).
42. Cerami, E. et al. The cBio cancer genomics portal: An open platform for exploring multidimensional cancer genomics data. *Cancer Discov.* **2**, 401–404. https://doi.org/10.1158/2159-8290.CD-12-0095 (2012).
43. Bardou, P., Mariette, J., Escudié, F., Djemiel, C. & Klopp, C. Jvenn: An interactive venn diagram viewer. *BMC Bioinform.* **15**, 293. https://doi.org/10.1186/1471-2105-15-293 (2014).
44. Kanehisa, M. & Goto, S. KEGG: Kyoto encyclopedia of genes and genomes. *Nucl. Acid. Res.* **28**, 27–30. https://doi.org/10.1093/nar/28.1.27 (2000).
45. Han, Y. et al. TISCH2: Expanded datasets and new tools for single-cell transcriptome analyses of the tumor microenvironment. *Nucleic Acids Res.* **51**, D1425-d1431. https://doi.org/10.1093/nar/gkac959 (2023).
46. Sun, X. et al. Comprehensive analysis of SLC35A2 in pan-cancer and validation of its role in breast cancer. *J. Inflamm. Res.* **16**, 3381–3398. https://doi.org/10.2147/JIR.S419994 (2023).

Author contributions

C.L. and C.S. designed the experiments; C.L., J.N. and Y.L. performed the experiments; C.L. and J.N. prepared all figures; C.L., J.N., Y.L., C.W. and W.L. analyzed the data; C.S. and B.S. supervised the work; C.L. wrote the manuscript.

Funding

This research was funded by the National Natural Science Foundation of China (No: 82560514) and the "Medical Excellence Award" funded by the Creative Research Development Grant from the First Affiliated Hospital of Guangxi Medical University.

Declarations

Competing interest

The authors declare no competing interests.

Ethics

The study received approval from the First Affiliated Hospital of Guangxi Medical University Ethics Committee (Approval No. 2024-S770-01). The written informed consent of the patient and/or their legal guardian was obtained before the tissue specimens were obtained. All animal experiments were conducted under the approval and supervision of the Ethics Committee of the First Affiliated Hospital of Guangxi Medical University (approval number: 2024-D0291).

Additional information

Supplementary Information The online version contains supplementary material available at https://doi.org/10.1038/s41598-026-45826-1.

Correspondence and requests for materials should be addressed to B.S. or C.S.